https://doi.org/10.15407/ujpe70.11.805

PRASHANT SRIVASTAV, ADWITIYA YADAV, PRAMOD KUMAR YADAWA

Department of Physics, Prof. Rajendra Singh (Rajju Bhaiya) Institute of Physical Sciences for Study and Research, Veer Bahadur Singh Purvanchal University
(Jaunpur 222001, India; e-mail: srivastavprashant001@gmail.com, adwitiya94@gmail.com, pkyadawa@gmail.com)

THEORETICAL INVESTIGATION OF THE MECHANICAL, AND THERMOPHYSICAL PROPERTIES OF MECHANOLUMINESCENCE MATERIAL WITH PARTIAL REPLACEMENT OF Li IN $\mathbf{Li_xZn_{1-x}O:Nd^{3+}}$ $\mathbf{(0 \leq x \leq 0.44)}$

The present work explores the mechanical, thermophysical, ultrasonic, and elastic properties of a novel mechanoluminescence (ML) material $Li_xZn_{1-x}O:Nd^{3+}$ by Lennard-Jones potential model. The reported elastic and mechanical properties are in good agreement with the further theoretical consequences. The evaluated mechanical properties proclaimed the mechanical stability in the Li additive interval of $0 \leq x \leq 0.44$. Elastic properties, such as Young's modulus, bulk modulus, and shear modulus decrease with an increase in the Li concentration from 0 to 0.44. The elastic softening derived from atomic interaction in the covalent bonding, concludes that the elastic softening is promoted by the increase in the Li–O bonding with a weak covalent bonding as the Li concentration increases. As a result of evaluating the B/G and Poisson's ratio, it is predicted that $Li_xZn_{1-x}O:Nd^{3+}$ material possesses the brittle behavior from the Li additive interval of $0 \leq x \leq 0.44$. Finally, the thermal properties including heat capacity per unit volume (C_V) and Debye temperature (θ_D) are obtained. The coefficient of ultrasonic attenuation, attributed to both the thermoelastic relaxation process and the phonon-viscosity interaction process, has been systematically analyzed for hcp-structured $Li_xZn_{1-x}O:Nd^{3+}$ at room temperature. The divulged results of this analysis have been elucidated with the available results of hcp-structured $Li_xZn_{1-x}O:Nd^{3+}$ as well as with other hcp-structured materials.

K e y w o r d s: mechanoluminescence material, elastic properties, mechanical properties, ultrasonic properties, thermal properties.

1. Introduction

Mechanoluminescence (ML) refers to the emission of light from a material, when it is subjected to the mechanical stress or deformation. This unique phenomenon has attracted considerable attention due to its broad range of potential applications, including sensors, structural health monitoring, and optical devices. ML occurs through various processes such as bond breaking, dislocation motion, and generation of charge carriers during a mechanical deformation. These processes enable materials to exhibit the light emission in response to mechanical stimuli, making ML a valuable tool for understanding the behavior of materials under the stress and for

C i t a t i o n: Srivastav P., Yadav A., Yadawa P.K. Theoretical investigation of the mechanical, and thermophysical properties of mechanoluminescence material with partial replacement of Li in $Li_xZn_{1-x}O:Nd^{3+}$ $(0 \leq x \leq 0.44)$. *Ukr. J. Phys.* **70**, No. 11, 805 (2025). https://doi.org/10.15407/ujpe70.11.805.

developing novel materials that can optically respond to mechanical forces. The study of ML has evolved significantly in recent years, with expanding interest in both inorganic and organic compounds, such as semiconductors, polymers, and composites. These materials hold a great promise for next-generation technologies, where the integration of mechanical and optical responses can lead to enhanced functionality and performance in diverse applications. In 1999, the evolution proclaimed by C.N. Xu *et al.* [1] of reproducible ML also referred to as piezoluminescence or elastic ML, in $ZnS:Mn^{2+}$ and $SrAl_2O_4:Eu^{2+}$, asserts it as a significant strides in research community. This breakthrough provided a significant advancement in the development of ML materials and their application in non-destructive testing via the ML phenomenon [1], sparking further research into ML materials, their underlying mechanisms, and their potential applications.

Subsequent studies, such as those by Kawan *et al.*, explored the phase stability and mechanical properties of $Li_xZn_{1-x}O:Nd^{3+}$ with a wurtzite structure [2–6] using first-principles calculations. Their work revealed enhanced near-infrared (NIR) ML characteristics in ZnO doped with Nd^{3+}, with the inclusion of Li^+ ions in the $ZnO:Nd^{3+}$ matrix resulting in an increase in the ML intensity in the NIR region. This enhancement underlined the importance of understanding the mechanisms behind the improved ML properties of $Li_xZn_{1-x}O:Nd^{3+}$ and highlighted its potential for a further development in the ML-based applications. A particular subset of ML, known as piezoluminescence, is observed during the elastic deformation of piezoelectric ML materials. These materials exhibit mechano-electro-optoelectronic conversion and are capable of undergoing multiple ML emission cycles in response to repetitive dynamic loads. The ability to detect and analyze piezoluminescence has immense potential for applications in both engineering and medicine [7–12]. The integration of piezoluminescent sensors into systems for remote wireless detection and analysis positions these materials as promising candidates for the stress-sensing and damage diagnosis technologies. It is well established that the ML intensity is proportional to strain [13]. When an external stimulus is applied to an ML material, its crystal lattice becomes distorted, resulting in the release of trapped charge carriers, which subsequently leads to the ML emission. In the case of $Li_xZn_{1-x}O:Nd^{3+}$, it is hypothesized that the higher ML intensity compared to pure $ZnO:Nd^{3+}$ can be attributed to two main factors. First, the incorporation of Li^+ ions into the ZnO structure may increase the number of trapped carriers within crystallographic defects. Second, the elasticity effect induced by the Li doping could alter the material's elastic constants, potentially modifying its piezoelectric properties and contributing to enhanced ML characteristics. The piezoelectric field generated by an external stress in the ML material could lead to the carrier de-trapping and electron acceleration, which, in turn, excites luminescent centers, resulting in the light emission.

This process is commonly referred to as the piezoelectricity-induced carrier de-trapping model, which has been observed in materials such as $ZnS:Mn^{2+}$ and (Ba, Ca) $^4TiO_3:Pr^{3+}$ [14]. In this study, we will focus on investigating the elastic, mechanical, and ultrasonic properties of $Li_xZn_{1-x}O:Nd^{3+}$ using Lennard–Jones potential model. The insights gained from this research will contribute significantly to future studies of the mechanical properties of $Li_xZn_{1-x}O:Nd^{3+}$, offering a deeper understanding of its fundamental characteristics. Moreover, the comparison of elastic and ultrasonic coefficients in this material will further enhance our understanding of its behavior and potential for ML-based applications.

2. Theory

The higher-order elastic coefficients (HOECs) are essential variables, as they connect the several thermophysical features that help us to elucidate the condensed performance of the material. The basic interaction potential model approach is used to compute the higher-order nonlinear elastic coefficients to analyze the characteristics and properties of the materials. In this model, Lennard–Jones potential like a potential for several body interactions and the subsequent formulas are used to determine the second-order elastic constants (SOECs) and third-order elastic constants (TOECs) of the material with HCP structure [15, 16] as follows:

$$C_{11} = 24.1p^4C',\ C_{12} = 5.918p^4C',\ C_{13} = 1.925p^6C',$$
$$C_{33} = 3.464p^8C',\ C_{44} = 2.309p^4C',\ C_{66} = 9.851p^4C', \quad (1)$$

$$C_{111} = 126.9p^2B + 8.852p^4C',\ C_{133} = 3.695p^6B,$$
$$C_{112} = 19.168p^2B - 1.61p^4C',\ C_{144} = 2.309p^4B,$$
$$C_{113} = 1.924p^4B + 1.155p^6C',\ C_{155} = 1.539p^4B, \quad (2)$$
$$C_{123} = 1.617p^4B - 1.155p^6C',\ C_{333} = 5.196p^8B,$$
$$C_{222} = 101.039p^2B + 9.007p^4C',\ C_{344} = 3.464p^6B,$$

The harmonic parameter (χ) and enharmonic constraint (ψ) are obtained using the $'a'$ (basal plane distance), and $'p = c/a'$ (axial ratio) using the equations given by:

$$\chi = \frac{n(n-m)b_0}{8a^{n+4}} \text{ and } \psi = -\frac{\chi}{6a^2(m+n+6)}. \quad (3)$$

The SOECs under the Voigt–Reuss–Hill (VRH) approximation [17] is well-known to compute various mechanical parameters, such as Young's modulus (Y), shear modulus (G), Poisson's ratio (σ), Pugh's ratio (B/G), and bulk modulus (B) of the material [18]. Using the VRH approximation, the expressions for the bulk modulus and shear modulus are provided as:

$$M = C_{11} + C_{12} + 2C_{33} - 4C_{13}, \quad (4)$$

$$C^2 = (C_{11} + C_{12})C_{33} - 4C_{13} + C_{13}^2, \quad (5)$$

$$B_R = \frac{C^2}{M}; \quad B_V = \frac{2(C_{11} + C_{12}) + 4C_{13} + C_{33}}{9}, \quad (6)$$

$$G_V = \frac{M + 12(C_{44} + C_{66})}{30}, \quad (7)$$

$$G_R = \frac{5C^2C_{44}C_{66}}{2[3B_VC_{44}C_{66} + C^2(C_{44}C_{66})]}, \quad (8)$$

$$Y = \frac{9GB}{G + 3B}; \quad B = \frac{B_V + B_R}{2}, \quad (9)$$

$$G = \frac{G_V + G_R}{2}; \quad \sigma = \frac{3B - 2G}{2(3B + G)}. \quad (10)$$

The longitudinal (V_L) and two shear acoustical velocities of wave (V_{S1}, V_{S2}) are closely related to the SOECs and material density, and exist in hexagonally arranged materials. The formulation of these velocities are expressed as follows: [19]

$$V_L = \Big[\Big(C_{33}\cos^2\theta + C_{11}\sin^2\theta + C_{44} + [\{C_{11}\sin^2\theta -$$
$$- C_{33}\cos^2\theta + C_{44}(\cos^2\theta - \sin^2\theta)\}^2 +$$
$$+ 4\cos^2\theta\sin^2\theta(C_{13} + C_{44})^2]^{1/2}\Big)/(2\rho)\Big]^{1/2}, \quad (11)$$

$$V_{S1} = \Big[\Big(C_{33}\cos^2\theta + C_{11}\sin^2\theta + C_{44} - [\{C_{11}\sin^2\theta -$$
$$- C_{33}\cos^2\theta + C_{44}(\cos^2\theta - \sin^2\theta)\}^2 +$$
$$+ 4\cos^2\theta\sin^2\theta(C_{13} + C_{44})^2]^{1/2}\Big)/(2\rho)\Big]^{1/2}, \quad (12)$$

$$V_{S2} = \left[\frac{2C_{44}\cos^2\theta + (C_{11} - C_{12})\sin^2\theta}{2\rho}\right]^{1/2}. \quad (13)$$

The longitudinal wave, quasi-shear wave, and shear wave velocities are represented by the variables V_L, V_{S1}, and V_{S2}. The values ρ and θ represent the material's density and angle for the crystal's unique axis, or z-axis. We will use the following expressions [20,21] to find the density of the hexagonal structured material, given by:

$$\rho = \frac{2Mn}{3\sqrt{3}a^2cN_{\mathrm{A}}}. \quad (14)$$

Molecular weight, Avogadro number, and number of atoms per unit cell are represented by the symbols M, N_{A}, and n, correspondingly. Considering the Debye average velocity is interconnected to the elastic coefficients using V_L, V_{S1}, and V_{S2}, it is an essential measure in low-temperature physics. In favor of a wave propagation at any angle with the z-axis, the Debye average velocity (V_{D}) has been defined as [22, 23]

$$V_{\mathrm{D}} = \left[\frac{1}{3}\left(\frac{1}{V_L^3} + \frac{1}{V_{S1}^3} + \frac{1}{V_{S2}^3}\right)\right]^{-1/3}. \quad (15)$$

The Debye temperature (θ_{D}) of the material is influenced by the Debye average velocity (V_{D}). The Debye average velocity expressed is directly related to a variations in the Debye temperature [24].

$$\theta_{\mathrm{D}} = \frac{\hbar V_{\mathrm{D}}(6\pi^2N_{\mathrm{A}})^{1/3}}{k_{\mathrm{B}}}. \quad (16)$$

Here, the Boltzmann Constant is symbolized by k_{B}, the atom concentration is denoted by N_{A}, and the quantum of action, $\hbar$, is defined as Planck's constant alienated by 2π. The thermal distribution of phonons occurs during the ultrasonic wave passing. The thermal relaxation time (τ), which can be calculated using the following formula, is the duration of time expected for the thermal phonons to return to equilibrium [25]:

$$\tau = \tau_S = \frac{\tau_L}{2} = \frac{3k}{C_V V_{\mathrm{D}}^2} \quad (17)$$

k in this case signifies the thermal conductivity. The compound thermal conductivity [26] can be determined through:

$$k = k_{\mathrm{B}} V_{\mathrm{D}} \left(\frac{M}{n\rho N_{\mathrm{A}}}\right)^{-2/3}. \tag{18}$$

The total consequence of the ultrasonic attenuation $(\alpha/f^2)_{\mathrm{Total}}$, caused by the thermoelastic loss and Akhieser losses exhibited in the longitudinal (V_L), shear mode of propagation can be calculated as [27]:

$$(\alpha)_{\mathrm{Long}} = \frac{2\pi^2 f^2}{\rho V_L^3}\left[\frac{4}{3}\eta_e + \chi\right], \tag{19}$$

$$(\alpha)_{\mathrm{Shear}} = \frac{2\pi^2 f^2}{\rho V_s^3}\eta_e, \tag{20}$$

where $'f'$ seems to be the acoustic wave's frequency, ρ is the density of hcp metal, η_e is the viscosity due to the electron, and χ is the viscosity due to compression. Thermo-elastic loss and Akhiezer-type loss are mutually important for acoustic wave attenuation. The mathematical equation which is shown below describes the attenuation due to the Akhiezer loss obtained by [28]:

$$(\alpha/f^2)_{\mathrm{Akh}} = \frac{4\pi^2 \tau E_0 (D/3)}{2\rho V^3}. \tag{21}$$

Thermodynamically generated energy density is denoted by E_0, whereas the ultrasound wave's frequency is denoted by f. The mathematical expression which is given below considers the thermo-elastic loss $(\alpha/f^2)_{\mathrm{Th}}$:

$$(\alpha/f^2)_{\mathrm{Th}} = 4\pi^2 \langle \gamma_i^j \rangle^2 \frac{kT}{2\rho V_L^5}. \tag{22}$$

The following equation gives the total ultrasonic attenuation as:

$$\left\{\frac{\alpha}{f^2}\right\}_{\mathrm{Total}} = \left\{\frac{\alpha}{f^2}\right\}_{\mathrm{Th}} + \left\{\frac{\alpha}{f^2}\right\}_{\mathrm{Long}} + \left\{\frac{\alpha}{f^2}\right\}_{\mathrm{Shear}}, \tag{23}$$

where, $\left\{\frac{\alpha}{f^2}\right\}_{\mathrm{Th}}$ is the thermo-elastic loss, and $\left\{\frac{\alpha}{f^2}\right\}_{\mathrm{Long}}$ and $\left\{\frac{\alpha}{f^2}\right\}_{\mathrm{Shear}}$ are the ultrasonic attenuation coefficients for a longitudinal wave (V_L) and shear waves, correspondingly.

3. Result and Conclusion

3.1. Elastic and mechanical parameters

In the present work, we have computed the elastic coefficients (Six-SOECs and Ten-TOECs) by an interaction potential model and lattice characteristics for the $\mathrm{Li}_x\mathrm{Zn}_{1-x}\mathrm{O}:\mathrm{Nd}^{3+}$ Mechanoluminescence Material, "a" (lattice parameter) and c/a (axial ratio) [29]. The variation of lattice parameters are delinated in Fig. 1. The value of Lennard–Jones parameter (b_0) for $\mathrm{Li}_x\mathrm{Zn}_{1-x}\mathrm{O}:\mathrm{Nd}^{3+}$ under Li concentrations of $0.00 \le x \le 0.44$ are taken 2.25×10^{-64}, 1.9×10^{-64}, 1.49×10^{-64} and 1.135×10^{-64} erg$\cdot$cm^7. The values of the higher-order elastic coefficients (second and third-order) of the $\mathrm{Li}_x\mathrm{Zn}_{1-x}\mathrm{O}:\mathrm{Nd}^{3+}$ Mechanoluminescence Material under Li concentrations of $0.00 \le x \le 0.44$ are obtained in Table 1 and Fig. 2 accordingly.

Elastic parameters can also improve knowledge of macroscopic mechanical characteristics and contribute to evaluating a material's hardness. In Table 1, the measurement value of C_{12}, C_{13}, C_{44}, and C_{66} decreases slightly less, while the value of C_{11} and C_{33} decreases with increasing the Dopant Concentration. Figure 2 illustrates the evaluated TOEC values with the Li additive range of $0 \le x \le 0.44$. TOECs with negative values signify strain within the solid. As a result, the model used to investigate higher-order elastic coefficients is acceptable using Eqs. (1), (2). For HCP structure material stability, the five different SOECs (C_{ij}, namely C_{11}, C_{12}, C_{13}, C_{33}, C_{44}) satisfy the Born–Huang's

Table 1. **Variation of SOECs in $\mathrm{Li}_x\mathrm{Zn}_{1-x}\mathrm{O}:\mathrm{Nd}^{3+}$ with dopant concentration**

Concentration x		C_{11}	C_{12}	C_{13}	C_{33}	C_{44}	C_{66}
0	Present Work	184.39	45.279	39.13	187.09	46.94	72.31
	[29]	184.1	104.4	91.9	186.4	39.0	–
0.11	Present Work	165.44	40.625	35.11	167.85	42.11	64.88
	[29]	166.1	95.0	80.5	167.4	34.7	–
0.22	Present Work	134.57	33.05	28.21	133.22	33.84	52.77
	[29]	138.1	79.0	60.8	133.3	30.9	–
0.33	Present Work	125.56	30.83	25.99	121.25	31.18	49.23
	[29]	124.6	73.3	61.2	121.3	23.2	–
0.44	Present Work	97.82	24.02	18.77	81.15	22.51	38.36
	[29]	118.2	71.7	59.7	81.3	20.8	–

norms [30]. This $Li_xZn_{1-x}O:Nd^{3+}$ Mechanoluminescence Material is mechanically stable at the Li additive range of $0 \leq x \leq 0.44$ because it is evident that the positive elastic constant values satisfy Born–mechanical Huang's stability constraints. The hcp material $Li_xZn_{1-x}O:Nd^{3+}$shear modulus (G), Young's modulus (Y), toughness (G/B), bulk modulus (B), Pugh's ratio (B/G), and Poisson ratio (σ) with the Li additive interval of $0 \leq x \leq 0.44$ have been calculated and shown in Table 2.

The values of B, Y, and G for $Li_xZn_{1-x}O:Nd^{3+}$ are observed to decrease with increasing the additive amount of Li. These negative correlations between the elastic properties and the additive amount of Li indicate an elastic softening behavior due to the Li addition. We have verified that Young's modulus (Y) is 151 GPa, the shear modulus (G) is 61 GPa, and the bulk modulus (B) is 94 GPa, which is consistent with experimental results for ZnO single crystal ($Y = 114$ GPa, $G = 42$ GPa, $B = 114$ GPa)[31].

This indicates that $Li_xZn_{1-x}O:Nd^{3+}$ Mechanoluminescence Material has relatively higher stiffness and bonding strength. The ratio of G/B indicates that if it is about 0.6, the compound consists mainly of ionic bonds. This ratio helps us to predict the bonding unique features of compounds as well as ratios B/G and σ provide insights into the materials' brittleness and ductility. Materials with $\sigma = 0.23 \leq$ ≤ 0.26 and $B/G = 1.52 \leq 1.75$ are typically considered brittle, or else they are ductile in nature. Our results for B/G indicate that $Li_xZn_{1-x}O:Nd^{3+}$ Material is brittle at the Li additive interval of $0 \leq x \leq 0.44$, because they are at their critical levels. The value of σ which should perfectly be less than 0.5 for elastic and stable metal, is found to be within an acceptable interval for $Li_xZn_{1-x}O:Nd^{3+}$ material. The density of $Li_xZn_{1-x}O:Nd^{3+}$ Material decreases with increased the dopant concentration and the volume of the $Li_xZn_{1-x}O:Nd^{3+}$ material decreases with increasing the dopant concentration are shown in Fig. 3.

3.2. Ultrasonic velocity

Figures 4–7 show the angular correlations of ultrasonic velocities (V_L, V_{S1}, V_{S2}, V_D) at various concentrations along the z-axis of the $Li_xZn_{1-x}O:Nd^{3+}$ material In Figs. 4 and 5, the z-axis of the $Li_xZn_{1-x}O:Nd^{3+}$ correlates directly to the minima and maxima of the ultrasonic velocities V_L and V_{S1} of the $Li_xZn_{1-x}O:Nd^{3+}$. In Fig. 6, V_{S2} rises through the angle away along the z-direction. The combined effects of SOECs and ρ (density) are held responsible

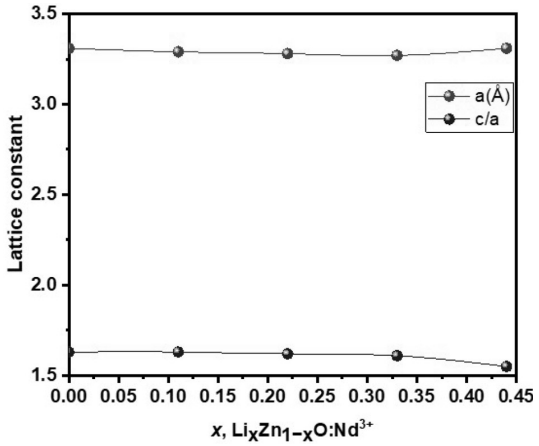

Fig. 1. Variation of lattice parameter in $Li_xZn_{1-x}O:Nd^{3+}$ with dopant concentration

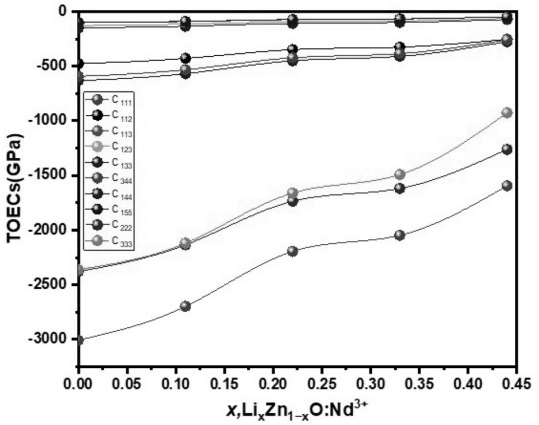

Fig. 2. Variation of TOECs in $Li_xZn_{1-x}O:Nd^{3+}$ with dopant concentration

Table 2. **Voigt–Reuss' constants (M and C^2), B (in 10^{10} Nm^{-2}), G (in 10^{10} Nm^{-2}), Y (in 10^{10} Nm^{-2}), G/B, B/G, and σ of $Li_xZn_{1-x}O:Nd^{3+}$ with dopant concentration**

Concentration (x)	M	C^2	B	G	Y	G/B	B/G	σ
0	447	44343	94	61	151	0.6	1.5	0.23
0.11	401	35680	84	55	136	0.6	1.5	0.23
0.22	321	23013	68	44	109	0.6	1.5	0.23
0.33	294	19533	63	41	101	0.6	1.5	0.23
0.44	209	10164	46	30	75	0.6	1.5	0.23

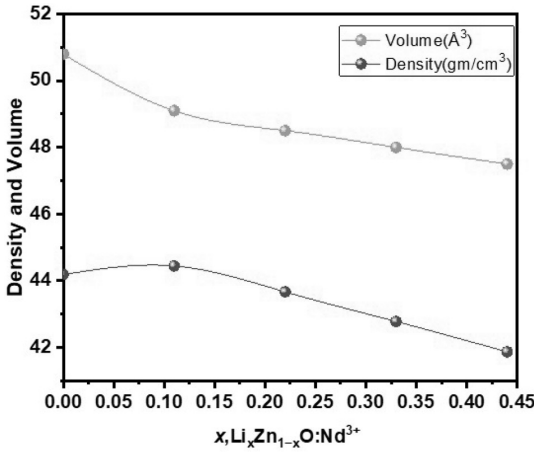

Fig. 3. Variation of volume and density in $\mathrm{Li}_x\mathrm{Zn}_{1-x}\mathrm{O}:\mathrm{Nd}^{3+}$ with dopant concentration

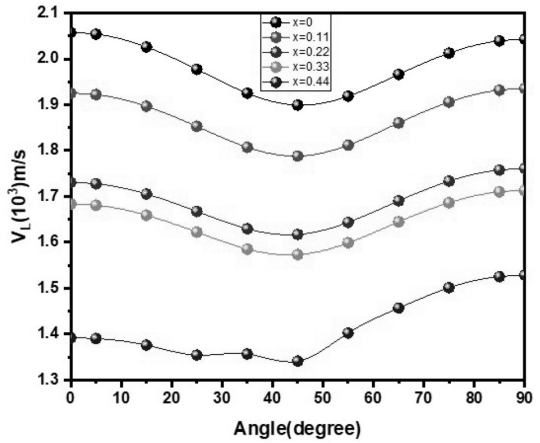

Fig. 4. Variation of angle-dependent ultrasonic velocity (V_L) in $\mathrm{Li}_x\mathrm{Zn}_{1-x}\mathrm{O}:\mathrm{Nd}^{3+}$ with dopant concentration

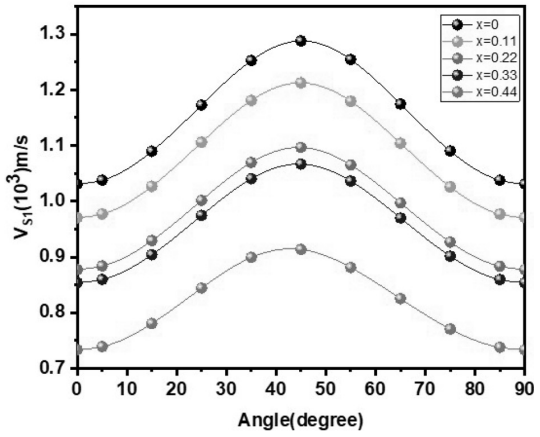

Fig. 5. Variation of angle-dependent ultrasonic velocity (V_{S1}) in $\mathrm{Li}_x\mathrm{Zn}_{1-x}\mathrm{O}:\mathrm{Nd}^{3+}$ with dopant concentration

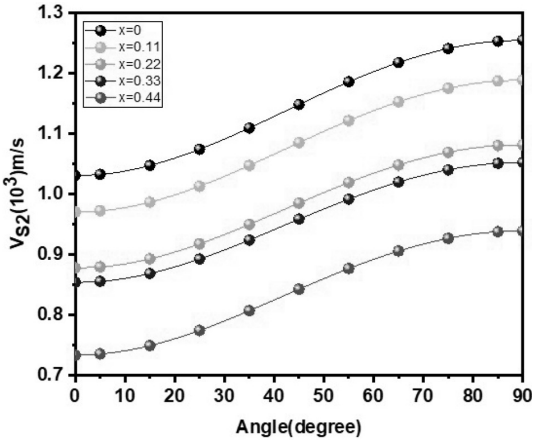

Fig. 6. Variation of angle-dependent ultrasonic velocity (V_{S2}) in $\mathrm{Li}_x\mathrm{Zn}_{1-x}\mathrm{O}:\mathrm{Nd}^{3+}$ with dopant concentration

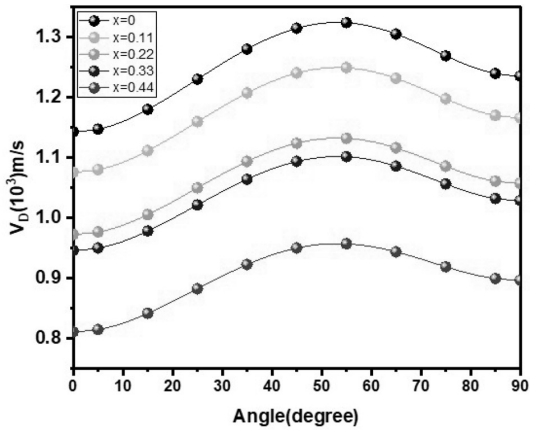

Fig. 7. Variation of angle-dependent ultrasonic velocity V_D in $\mathrm{Li}_x\mathrm{Zn}_{1-x}\mathrm{O}:\mathrm{Nd}^{3+}$ with dopant concentration

in favor of the uncharacteristic behavior of θ (angle) dependent velocity [32]. The existence of an angle (θ)-dependent velocities (V) curve in this effort is comparable to that used for the other HCP material. Hence, the θ- dependence of the velocities in the material is acceptable.

Figure 7 shows the variance of the Debye average velocity (V_D) as depends upon θ with the unique axis. V_D is accomplished when utilizing the ultrasonic velocities V_L, V_{S1}, and V_{S2} for $\mathrm{Li}_x\mathrm{Zn}_{1-x}\mathrm{O}:\mathrm{Nd}^{3+}$ material. Its maximum value reaches 55° and it increases with angle (θ).

3.3. Thermal properties

Using Eq. (18), the considered κ values of $\mathrm{Li}_x\mathrm{Zn}_{1-x}\mathrm{O}:\mathrm{Nd}^{3+}$ with dopant concentration are ob-

tainable in Fig. 8. From Fig. 8, it is understandable that k of $Li_xZn_{1-x}O:Nd^{3+}$ decreases with increasing the dopant Concentration The obtained C_V values of $Li_xZn_{1-x}O:Nd^{3+}$ with dopant concentration exist in Fig. 9. C_V value of $Li_xZn_{1-x}O:Nd^{3+}$ increases with increasing dopant concentration is obtained in Fig. 9. In Fig. 9, the E_0 increases with increasing the dopant concentration. Since the Debye temperature and specific heat per unit volume have opposite correlations, Figure 10 illustrates their opposing nature. The energy density (E_0) has been considered with $\frac{\theta_D}{T}$ table of AIP handbook [33] and is obtainable in Fig. 9. The angle and dopant concentration-dependent on the $'\tau'$ (thermal relaxation) is considered through Eq. (17).

The angle and concentration dependence on the thermal relaxation time are obtained in Fig. 10. In Fig. 10, the thermal relaxation time is of order of 10–12 ps. This indicates that $Li_xZn_{1-x}O:Nd^{3+}$ is intermetallic hexagonal. Thus, the thermal conductivity ($\tau \propto k$) has a definite impact on $Li_xZn_{1-x}O:Nd^{3+}$ thermal relaxation time. P–P (phonon-phonon) interaction and τ thermal relaxation processes induce ultrasonic attenuation, as demonstrated by the shortest computation time for the thermal phonon equilibrium distribution for wave propagation ($\theta = 50°$).

3.4. Ultrasonic attenuation based on thermal relaxation events and phonon-phonon (p-p) interaction

In analyzing the $\left\{\frac{\alpha}{f^2}\right\}_{\text{Th}}$ ultrasonic attenuation, it was assumed that the waves flow all along the z-axis of $Li_xZn_{1-x}O:Nd^{3+}$ material.

Attenuation coefficients alienated over frequency squared (α^2) for $\left\{\frac{\alpha}{f^2}\right\}_{\text{Long}}$ (longitudinal wave) and for $\left\{\frac{\alpha}{f^2}\right\}_{\text{Shear}}$ (shear wave) under condition $\alpha\tau < 1$

Table 3. $\left\{\frac{\alpha}{f^2}\right\}_{\text{Th}}$, $\left\{\frac{\alpha}{f^2}\right\}_{\text{Long}}$, $\left\{\frac{\alpha}{f^2}\right\}_{\text{Shear}}$ and $\left\{\frac{\alpha}{f^2}\right\}_{\text{Total}}$ of $Li_xZn_{1-x}O:Nd^{3+}$ with dopant concentration

Concentration (x)	$\left\{\frac{\alpha}{f^2}\right\}_{\text{Th}}$ (10^{-20}) $\text{Nps}^2\text{m}^{-1}$	$\left\{\frac{\alpha}{f^2}\right\}_{\text{Long}}$ (10^{-18}) $\text{Nps}^2\text{m}^{-1}$	$\left\{\frac{\alpha}{f^2}\right\}_{\text{Shear}}$ (10^{-20}) $\text{Nps}^2\text{m}^{-1}$	$\left\{\frac{\alpha}{f^2}\right\}_{\text{Total}}$ (10^{-20}) $\text{Nps}^2\text{m}^{-1}$
0	2.194	25.656	2.153	27.809
0.11	2.801	32.522	2.729	35.251
0.22	4.420	52.871	4.088	56.959
0.33	5.306	63.566	4.816	68.382
0.44	11.432	140.318	18.956	159.227

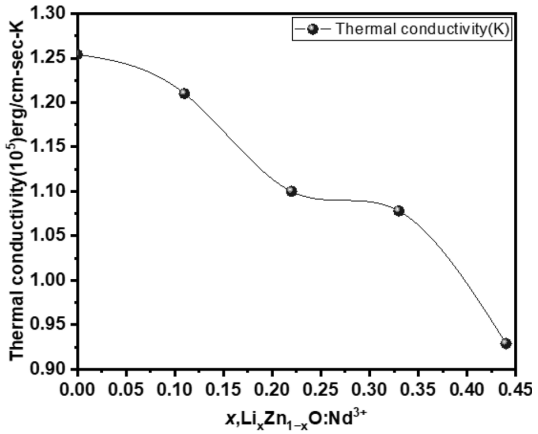

Fig. 8. Thermal conductivity ($k_{\min}$) variation in $Li_xZn_{1-x}O:Nd^{3+}$ with dopant concentration

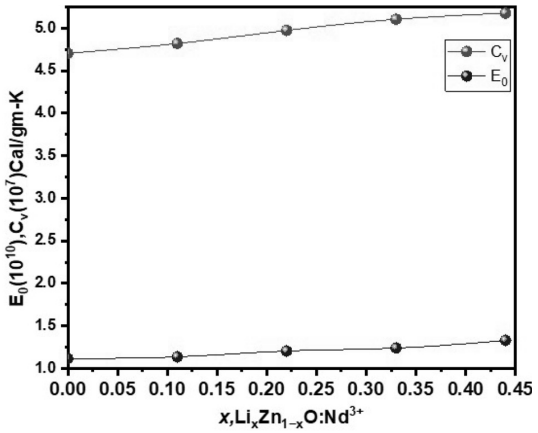

Fig. 9. Variation of the specific heat per unit volume (C_V) and energy density (E_0) in $Li_xZn_{1-x}O:Nd^{3+}$ with dopant concentration

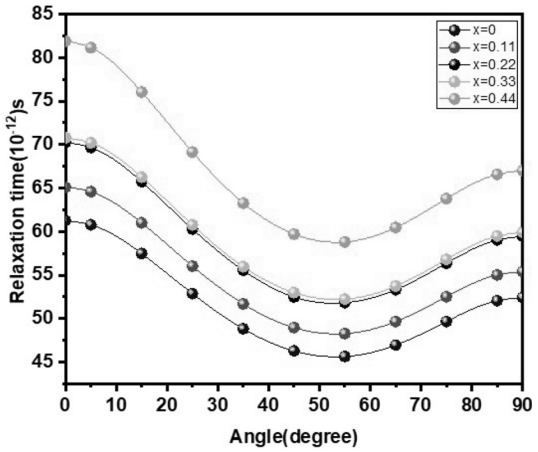

Fig. 10. Variation of angle-dependent relaxation time in $Li_xZn_{1-x}O:Nd^{3+}$ with dopant concentration

at dopant concentration is calculated using Eq. (19) and obtained in Table 3. The thermo-elastic loss by frequency squared $\left\{\frac{\alpha}{f^2}\right\}_{\mathrm{Th}}$ is calculated using Eq. (22), and the Table 3 illustrates the ultrasonic attenuation value resulting from the thermo-elastic relaxation mechanism $\left\{\frac{\alpha}{f^2}\right\}_{\mathrm{Th}}$.

The $\left(\frac{\alpha}{f^2}\right)_{\mathrm{Akh}} \propto \mathrm{D}$, E_0 and V^{-3} using Eq. (21). Thus, in the $\mathrm{Li}_x\mathrm{Zn}_{1-x}\mathrm{O}:\mathrm{Nd}^{3+}$ material, E_0 and K have a considerable impact on Akhieser losses. The results of $(\alpha/f^2)_{\mathrm{Akh}}$ have been compared through our recent studies. The thermo-elastic loss for the $\mathrm{Li}_x\mathrm{Zn}_{1-x}\mathrm{O}:\mathrm{Nd}^{3+}$ material is shown in Table 3 to be substantially less than the Akhieser loss, indicating that the p-p interaction mechanism-induced ultrasonic attenuation dominates over the thermo-elastic loss. Total attenuation is essentially driven by two variables, namely, thermal energy density and thermal conductivity. Thus, $\mathrm{Li}_x\mathrm{Zn}_{1-x}\mathrm{O}:\mathrm{Nd}^{3+}$ material is ductile.

4. Conclusion

Based on the above discussion, the following conclusions are drawn:

• The standard calculation technique for higher-order elastic coefficients for hexagonal $\mathrm{Li}_x\mathrm{Zn}_{1-x}\mathrm{O}:\mathrm{Nd}^{3+}$ material, based on the Lenard-Jones potential model, remains applicable for Li additive interval of $0 \leq x \leq 0.44$.

• $\mathrm{Li}_x\mathrm{Zn}_{1-x}\mathrm{O}:\mathrm{Nd}^{3+}$ material exhibits outstanding mechanical properties at room temperature.

• The stiffness and elastic constants of $\mathrm{Li}_x\mathrm{Zn}_{1-x}\mathrm{O}:\mathrm{Nd}^{3+}$ are observed to be superior to those of other mechanoluminescent materials. Analysis of the bulk modulus (B) and shear modulus (G), about their critical values, indicates that the incorporation of lithium induces a brittle-to-ductile transition as the Li content increases. In comparison with other mechanoluminescent materials, $\mathrm{Li}_x\mathrm{Zn}_{1-x}\mathrm{O}:\mathrm{Nd}^{3+}$ demonstrates a predominantly brittle behavior at room temperature.

• The relaxation time $'\tau'$ of $\mathrm{Li}_x\mathrm{Zn}_{1-x}\mathrm{O}:\mathrm{Nd}^{3+}$ material is established to the order of picoseconds, defending its inter-metallic nature. The smallest significance of $'\tau'$ along $= 50°$ at all temperatures indicates that the time required to re-establish the equilibrium distribution of phonons for wave propagation in the z-direction will be the shortest.

• Over the total ultrasonic attenuation caused by the p-p interaction mechanism is a governing factor of the thermal conductivity. The mechanical properties of $\mathrm{Li}_x\mathrm{Zn}_{1-x}\mathrm{O}:\mathrm{Nd}^{3+}$ mechanoluminescent material within the Li additive intercal of $x = 0$ are better than those within the intercal $0 \leq x \leq 0.44$. This enhancement in mechanical properties at $x = 0$ is attributed to the relatively low ultrasonic attenuation observed at this composition.

The current study investigates the nonlinear phenomena and anharmonic properties of mechanoluminescent materials. This work provides new insights and may catalyze future experimental investigations into the anharmonic characteristics of such materials. The findings of this study contribute valuable knowledge that could support further research endeavors and facilitate the development of industrial applications of mechanoluminescent materials.

5. Declaration of Competing Interest

The authors declare that they have no known competing financial interests or personal relationships that could have appeared to influence the work reported in this paper.

We have benefited immensely from the help and discussions with Mr. Vivek Kumar Srivastava, Department of Physics, Prof. Rajendra Singh (Rajju Bhaiya) Institute of Physical Sciences for Study and Research, Veer Bahadur Singh Purvanchal University, Jaunpur 222001, India. Authors are thankful to Center of Excellence grant from Department of Higher Education, Uttar Pradesh for financial support.

1. C.N. Xu, T. Watanabe, M. Akiyama, X.G. Zheng. Direct view of stress distribution in solid by mechanoluminescence. *Appl. Phys. Lett.* **74**, 2414-16 (1999).
2. D. Tu, C.N. Xu, S. Kamimura, Y. Horibe, H. Oshiro, L. Zhang, Y. Ishii, K. Hyodo, G. Marriott, N. Ueno *et al.* Ferroelectric $\mathrm{Sr_3Sn_2O_7}:\mathrm{Nd}^{3+}$: A new multipiezo material with ultrasensitive and sustainable near-infrared piezoluminescence. *Adv. Matte.* **32** (25), 1908083 (2020).
3. X. Yang, R. Liu, X. Xu, Z. Liu, M. Sun, W. Yan, D. Peng. Effective repeatable mechanoluminescence in heterostructured $\mathrm{Li}_{1-x}\mathrm{Na}_x\mathrm{NbO_3}:\mathrm{Pr}^{3+}$. *Small* **17** (46), 2103441 (2021).
4. Y. Fujio, C.N. Xu, N. Terasaki. Flexible mechanoluminescent $\mathrm{SrAl_2O_4}:\mathrm{Eu}$ film with tracking performance of CFRP fracture phenomena. *Sensor* **22** (15), 5476 (2022).
5. D. Tu, C.N. Xu, A. Yoshida, M. Fujihala, J. Hirotsu, X.G. Zheng. $\mathrm{LiNbO_3}:\mathrm{Pr_{3+}}$: A multipiezo material with simultaneous piezoelectricity and sensitive piezoluminescence. *Adv. Matter.* **29** (22), 1606914 (2017).

6. J.C. Zhang, X. Wang, G. Marriott, C.N. Xu. Trapcontrolled mechanoluminescent materials. *Prog. Mater. Sci.* **103**, 678 (2019).
7. C. Feng, H. Zhang, Y. Deng, A. Y, X. Chen, J. Sun, M. Zhang, L. Dong. High wurtzite content ZnS : Mn with better luminescent performances prepared at lower temperature by a ball milling method. *J. Alloys. Compd.* **968**, 172211 (2023).
8. H. Hara, C.N. Xu, R. Wang. Control of crystal structure and performance evaluation of multi-piezo material of $Li_{1-x}Na_xNbO_3 : Pr^{3+}$. *J. Ceramic Society of Japan* **128** (8), 518 (2020).
9. P. Chandrakar, D.P. Bisen, R.N. Baghel, B.P. Chandra. Synthesis and optical properties of $CaMgSi_2O_6 : Ce^{3+}$ phosphors. *J. Electron. Mater.* **44**, 3450 (2015).
10. A. Feng, P.F. Smet. A review of mechanoluminescence in inorganic solids: Compounds, mechanisms, models and applications. *Materials* **11**, 484 (2018).
11. J. Sik, Y.N. Kwon, K.S. Sohn. Dynamic visualization of crack propagation and bridging strees using the mechanoluminescence of $SrAl_2O_4 : (Eu, Dy, Nd)$. *Acta Materialia* **51**, 6437 (2003).
12. S. Zhang, S. Wang, T. Hu, S. Xuan, H. Jiang, X. Gong. Study the safeguarding performance of shear thickening gel by the mechanoluminescence method. *Composites Part B* **180**, 107564 (2020).
13. Z.J. Wu, E.J. Zhao, H.P. Xiang, X.F. Hao, X.J. Liu, J. Meng. Crystal structures and elastic properties of superhard IrN_2 and IrN_3 from first principles. *Phys. Rev. B* **76**, 054115 (2007).
14. H. Pan, J. Zhang, X. Jia, H. Xing, J. He, J. Wang, F. Wen. Large electrostrictive effect and high optical temperature sensing in $Bi_{0.5}Na_{0.5}TiO_3$–$BaTiO_3$–$(Sr_{0.7}Bi_{0.18}Er_{0.02})$ TiO_3 luminescent ferroelectrics. *Ceramic International* **44** (5), 57859 (2018).
15. S. Rai, A.K. Prajapati, P.K. Yadawa. Effect of pressure on elastic constants and related properties of rare-earth intermetallic compound TbNiAl. *Phys. Mesomech.* **26**, 495 (2023).
16. S. Rai, N. Chaurasiya, P.K. Yadawa. Elastic, mechanical and thermophysical properties of single-phase quaternary ScTiZrHf high-entropy alloy. *Phys. Chem. Solid State* **22**, 687 (2021).
17. W. Voigt. *Lehrbuch der kristallphysik* (B G Teubner, 1910).
18. S.F. Pugh. Relations between the elastic moduli and the plastic properties of polycrystalline pure metals. *Philos. Mag.* **45**, 823 (1954).
19. A.K. Prajapati, S. Rai, P.K. Yadawa. Pressure dependent elastic, mechanical, thermo-physical and ultrasonic properties of titanium boride. *MAPAN* **37**, 597 (2022).
20. V. Rajendran, A. Marikani. *Materials Science* (Tata MC-Graw Hill education, 2009).
21. P.K. Yadawa, S. Rai, N. Chaurasiya, A.K. Prajapati. Investigation of intermetallic GdFeAl ternary compound by elastic, thermophysical and ultrasonic analysis. *Phys. and Astronomy* **19**, 105-12 (2022).
22. A.K. Prajapati, S. Rai, P.K. Yadawa.Theoretical investigations on mechanical and ultrasonic characteristics of gallium nitride semiconductor under high pressure. *Emergent Mater.* **5**, 1985 (2022).
23. P. Srivastav, A.K. Prajapati, P.K. Yadawa. Theoretical investigation on thermal, mechanical and ultrasonic properties of zirconium metal with pressure. *Phys. Chem. Solid State* **24**, 549-97 (2023).
24. S.O. Pillai. *Solid State Physics* (New age international publisher, 2021) [ISBN: 0025472570028].
25. D. Singh, D.K. Pandey, P.K. Yadawa. Ultrasonic wave propagation in rare-earth monochalcogenides. *Centr. Eur. J. Phy.* **7**, 198 (2009).
26. D.R. Clarke. Materials selection guidelines for low thermal conductivity thermal barrier coatings. *Surf. Coat. Technol.* **163**, 67 (2003).
27. R.P. Singh, S. Yadav, G. Mishra, D. Singh. Pressure dependent ultrasonic properties of hcp hafnium metal. *Zeitschrift für Naturforschung.* **7**, 549 (2021).
28. A.K. Gupta, A. Gupta, S. Tripathi, V. Bhalla, D. Singh. Ultrasonic properties of hexagonal closed packed metals. *Universal J. Mater. Sci.* **1**, 63 (2013).
29. S. Kawana, K. Hirata, Y. Fujio, T. Uchiyama, C.N. Xu. First-principles calculation of elastic properties in $Li_xZn_{1-x}O : Nd$ mechanoluminescence material. *Advanced Theory and Simulations* **7**, 2400099 (2024).
30. S. I. Ranganathan, M. Ostoja-starzewski. Universal elastic anisotropy index. *Phys. Rev. Lett.* **101**, 9007-08 (2008).
31. T. Azuhata, M. Takesada, T. Yagi, A. Shikanai, S.F. Chichibu, K. Torii, A. Nakamura, T. Sota, G. Cantwell, C.W. Litton. Brillouin scattering study of ZnO. *J. Appl. Phys.* **94**, 968 (2003).
32. S. Berri. First-principles calculations to investigate structural, electronic,half-metallic and thermodynamic properties of hexagonal UX_2O_6 (X = Cr,V) compounds. *J. Sci. Adv. Mater. Devices* **4**, 319 (2019).
33. D.E. Gray. *AIP Handbook*, 3rd ed. (Mc-Graw Hill Book Co. Inc., 1965) [ISBN: 2674298170].

Received 05.04.25

П. Срівастав, А. Ядав, П.К. Ялава

ТЕОРЕТИЧНЕ ДОСЛІДЖЕННЯ МЕХАНІЧНИХ ТА ТЕРМОФІЗИЧНИХ ВЛАСТИВОСТЕЙ МЕХАНОЛЮМІНЕСЦЕНТНОГО МАТЕРІАЛУ З ЧАСТКОВОЮ ЗАМІНОЮ Li В $Li_xZn_{1-x}O : Nd^{3+}$ $(0 \le x \le 0{,}44)$

У цій роботі досліджуються механічні, теплофізичні, ультразвукові та пружні властивості нового механолюмінесцентного матеріалу $Li_xZn_{1-x}O : Nd^{3+}$ на основі моделі з використанням потенціалу Леннарда-Джонса. Механічна стабільність матеріалу продемонстрована в інтервалі $0 \le x \le 0{,}44$ відносного вмісту Li. Такі параметри, як модуль Юнга, модуль об'ємної пружності та модуль зсуву зменшуються зі збільшенням концентрації Li від 0 до 0,44. Отримано питому теплоємність (C_V) і температуру Дебая (θ_D). Проаналізовано коефіцієнт ультразвукового затухання за кімнатної температури.

Ключові слова: механолюмінесцентний матеріал, пружні властивості, механічні властивості, ультразвук, термодинамічні властивості.